

Sub-milliwatt optical frequency combs in dual-pumped high-Q multimode silicon resonators

Yaojing Zhang, Keyi Zhong, Gaolei Hu, Dan Yi, Rakesh Ranjan Kumar, and Hon Ki Tsang^{a)}

Department of Electronic Engineering, The Chinese University of Hong Kong, Shatin, New Territories, Hong Kong

We experimentally study the generation of optical frequency combs (OFCs) in dual-pumped high-quality-factor ($>10^6$) multimode silicon racetrack resonators and showed that sub-milliwatt (0.3 mW) input pump powers were sufficient to produce six-order OFC generation with eleven peaks, even in waveguides with normal dispersion. The low pump power and enhanced efficiency of the OFC generation can be attributed to mode coupling between two mode families of the multimode resonator, which acts to change the effective magnitude and sign of the local dispersion of the resonator. We experimentally observed that the OFC generation had 3.6 times more peaks and 12.1 dB higher conversion efficiency than that without any bias. We compared the efficiencies of the OFC generation at different pump wavelengths within and beyond the mode coupling region. At low pump powers circulating in the resonator, pump wavelengths in the mode coupling regime produced 1.3 times more peaks and 8 dB enhancement in conversion efficiency than pumping beyond the mode coupling regime. The experimental results were consistent with the theoretical simulations by solving the modified Lugiato-Lefever equation.

Optical frequency combs (OFCs), based on the third-order optical nonlinear susceptibility, have a wide range of applications, including signal regeneration,¹ wavelength converters,² and optical time lens³. Highly efficient and broadband OFC generation usually requires anomalous dispersion to satisfy the phase-matching condition.⁴ The presence of normal dispersion would inhibit the modulation instability needed for the initiation of the frequency comb.⁵ However, recent work in silicon nitride microresonators has shown that mode coupling can change the local dispersion and thus enable the generation of OFCs in the normal dispersion regime of multimode resonators.⁵⁻⁸ This technique can aid the excitation of dark pulses in normal-dispersion microresonators.⁹ Generally, mode coupling arises when resonances from different modes families approach each other, and their interaction would shift the resonant frequencies and form hybrid modes, leading to local effective dispersion changes for the avoided modal crossing.^{7, 10} The avoided modal crossing acts to break the continuous dispersion of the fundamental mode of the microresonator.^{5, 11} In contrast, in the anomalous dispersion regime, mode coupling is detrimental to comb generation since it may inhibit the soliton formation and affect the comb spectrum^{12, 13}. The waveguide size and cross-section aspect ratio determine the dispersion. Typically, a silicon waveguide with a small cross-section area would have

^{a)} Author to whom correspondence should be addressed. Electronic mail: hktsang@ee.cuhk.edu.hk.

This is the author's peer reviewed, accepted manuscript. However, the online version of record will be different from this version once it has been copyedited and typeset.

PLEASE CITE THIS ARTICLE AS DOI: 10.1063/1.50025490

anomalous dispersion, while a large core size typically has normal dispersion.¹⁴ To achieve the phase-matching condition using anomalous dispersion, most of the previous work employed resonators with small core sizes. However, due to the large optical field overlap between the fundamental mode and the waveguide sidewalls, the resonators with narrower waveguides suffer from higher losses. The larger propagation loss would limit the quality factor (Q) of the resonator. Hence higher input pump power is typically needed for OFC generation.

Recent work on multimode waveguides has demonstrated their advantages for nonlinear devices. For example, a multimode silicon nitride resonator with a high Q of 3.7×10^7 supported parametric oscillation at sub-milliwatt pump powers.¹⁵ A multimode silicon resonator with a Q of 1.1×10^6 gave a high conversion efficiency in four-wave mixing (FWM).¹⁶ Intermodal FWM has been previously studied in multimode silicon waveguides.¹⁷ Multimode waveguides have also attracted recent attention for applications in integrated quantum photonics to produce photon pairs with high visibility entanglements and the generation of heralded single photons.^{18, 19} Taking advantage of the low-loss multimode waveguide, we previously reported initial experimental results on efficient FWM in a multimode silicon racetrack resonator.²⁰

In this paper, we use two pump lasers to drive a multimode silicon resonator. By exploiting its higher Q and mode coupling, we observed the generation of an OFC generation in the normal dispersion silicon resonator. We experimentally investigated the effects of different reverse bias voltages and pump wavelengths within and beyond the mode coupling region on the efficiency of the OFC generation in the silicon resonator. The multimode silicon waveguide was designed to have a low loss of 0.41 ± 0.16 dB/cm by using wide waveguides to reduce scattering losses. The multimode waveguide was used to construct a millimeter-scale racetrack resonator with a high Q of $\sim 1.8 \times 10^6$. By applying a reverse bias of 25 V, the pump power of FWM in the resonator was reduced from 132 μ W (without any bias) to 6 μ W. The waveguide has normal dispersion, but the mode coupling between two modes modified the local dispersion of the resonator and enabled the highly efficient six-order OFC generation with eleven peaks using coupled pump powers of only ~ 0.3 mW and 25 V reverse bias. The experimental results agreed well with the theoretical predictions by solving the modified Lugiato-Lefever equation.

FIG. 1. Schematic of the silicon racetrack resonator and simulated group-velocity dispersion. (a) Structure of the silicon racetrack resonator with zoom-in cross-section and the microscope image of the silicon racetrack resonator. Simulated fundamental mode is well confined in the waveguide. (b) Simulated group-velocity dispersion of the bus waveguide at wavelengths ranging from 1400 nm to 1700 nm, indicating normal dispersion.

The designed silicon racetrack resonator has a height of 220 nm, etch depth of 70 nm, and a width of 2 μ m is shown in FIG. 1. It was fabricated in a multi-project wafer shuttle run by *IMEC foundry* on a 220-nm thick silicon-on-insulator wafer. The bend radius of the racetrack resonator is 130 μ m, yielding a low bending loss for the multimode waveguide, and the straight

waveguide of the racetrack has a length of 1000 μm . A symmetric lateral p-i-n diode was fabricated with the waveguide to remove the free carriers produced by two-photon absorption (TPA) in the silicon waveguide. The light was coupled into and out of the bus waveguide via edge couplers and lens fibers, which allow for coupling with broadband wavelengths. As shown in FIG. 1, the simulated fundamental mode shows good confinement in the waveguide. The simulated group-velocity dispersion (GVD) of the bus waveguide is shown in FIG. 1b and the silicon waveguide has normal GVD from wavelengths of 1400 nm to 1700 nm.

FIG. 2. Transmission characteristics of the silicon resonator. (a) Transmission spectra with an input power of 0.1 mW and wavelength step of 0.1 pm. Upper spectrum at wavelengths from 1530 nm to 1580 nm with dashed boxes showing the mode coupling regions. The below spectrum is one zoom-in region. The 'x' marks represent the fundamental modes, and the '+' marks are the higher-order modes. In this region, the higher-order modes gradually get close to the fundamental modes and affect the local GVD of the resonator. And two resonant wavelengths around (b) 1560.27 nm and (c) 1560.51 nm.

We used a tunable laser with low power of 0.1 mW and a fine wavelength scanning with a step of 0.1 pm to measure the transmission spectra of the resonator, as shown in FIG. 2, from 1530 nm to 1580 nm. In FIG. 2a, the dashed boxes mark the mode coupling regions. Using wavelengths ranging from 1559 nm to 1563 nm as an example, the 'x' marks are the fundamental modes, while '+' marks indicate the higher-order modes. In the mode coupling region, as shown in FIG. 2a, the higher-order mode is first located on the long-wavelength side of the fundamental mode. As the laser is tuned to longer wavelengths, the relative position of the higher-order mode gradually approaches the fundamental mode resonance and moves to the short wavelength side of the fundamental mode resonance, as shown on the right side of FIG. 2a. The higher-order mode family affects the effective GVD of the fundamental mode family. This mechanism of mode coupling has been well studied in silicon nitride resonators.⁵⁻⁷ A more precise measurement of free spectral range (FSR) was previously reported using a frequency-comb-assisted spectroscopy method.¹¹ The insertion loss of the fiber-chip-fiber was first measured to be -4.7 dB. In the mode coupling region, we chose two resonances around 1560.27 nm and 1560.51 nm. The asymmetric Fano line shapes of the two resonances indicate the existence of the mode coupling.^{21,22} We measured the full width at half maximum (FWHM) linewidth as 0.95 pm and 0.86 pm, respectively. The loaded Qs of the two resonances were calculated as 1.6×10^6 and 1.8×10^6 , respectively. The corresponding enhancement factors were calculated to be 32.3 and 46.6. The FSR was measured to be 0.24 nm, as shown in FIG. 2. From $FSR = \lambda_{res}^2 / n_g L$ (λ_{res} is the resonant wavelength, n_g is the group index and L is the round-trip length),²³ we can calculate that the group index n_g is 3.6. For a resonator, the total propagation loss of the cavity can be calculated using:

$$\alpha = \frac{2\pi n_g}{Q_i \lambda_{res}} = \frac{\lambda_{res}}{Q_i \times FSR \times R}, \quad (1)$$

This is the author's peer reviewed, accepted manuscript. However, the online version of record will be different from this version once it has been copyedited and typeset.

PLEASE CITE THIS ARTICLE AS DOI: 10.1063/1.50025490

$$Q_i = \frac{2Q_L}{1 \pm \sqrt{T}}, \quad (2)$$

where R is the radius of the resonator, T is the normalized transmission at the resonance, and Q_L/Q_i is the loaded/intrinsic Q of the resonator.^{24,25} In the overcoupled regime, the equation takes the $-$ sign, while it has $+$ sign in undercoupled regime.²⁵ With the above equations, we calculated the propagation loss of the resonator to be 0.41 ± 0.16 dB/cm.

FIG. 3. Measured FWM spectra at pump wavelengths of 1560 nm (a) with a 25 V bias and (b) 0 V. The coupled pump powers were measured as $6 \mu\text{W}$ and $132 \mu\text{W}$.

Since mode coupling is known to affect the GVD of the resonators, we used the resonances around 1560.27 nm and 1560.51 nm to investigate the FWM behavior of the resonator in the mode coupling region. For the experimental setup, two tunable lasers indicated as pump 1 and pump 2 in FIG.3 were first adjusted to quasi-transverse-electric polarization by two polarization controllers. A 50/50 fiber coupler was used to combine the two pumps for coupling them into the waveguide using a lensed fiber and edge coupler. A source meter was used to apply the reverse bias and measured the direct current produced by TPA in the waveguide. The optical output was coupled into a 1:99 fiber coupler. 1% of the output power was monitored by a power meter, and an optical spectrum analyzer recorded the output spectrum. Application of a reverse bias of 25 V and pump powers set to only about $6 \mu\text{W}$ enabled the generation of the first side peak from FWM. The measured spectrum is shown in FIG. 3a. We conducted the same measurement without any bias and observed that the required pump powers increased to $132 \mu\text{W}$, as shown in FIG. 3b. There is about 20 times reduction of the pump power to generate the first FWM peak when the reverse bias of 25 V is applied. The conversion efficiency of the FWM is defined as the ratio of the first peak power relative to the pump 2 power. Including the loss of the resonator, the conversion efficiencies with the 25 V bias and 0 V bias were measured as -59.2 dB and -71.3 dB. There is a 12.1 dB enhancement in the conversion efficiency when the 25 V bias is applied. Because the 25 V reverse bias removes free carriers produced by TPA in the resonator, it reduces the optical loss and increases the conversion efficiency of the FWM.

FIG. 4. Measured OFCs spectra with reverse bias voltages of 25 V, 10 V, and 0 V and simulated OFCs spectrum with a reverse bias voltage of 25 V at pump wavelengths of 1560 nm. The coupled power of pump 1 was measured as 0.3 mW.

We further increased the pump power to investigate the effects of pump power and the bias voltage on the number of peaks and the conversion efficiency in the resonator. Due to the high Q factor of the resonator, the photocurrent from the source meter is very sensitive to the fine-tuning of the input wavelengths and enabled precise matching of the wavelengths to the respective resonances at different input powers. For the measurement of the OFC, we used two input pumps from two tunable lasers and

This is the author's peer reviewed, accepted manuscript. However, the online version of record will be different from this version once it has been copyedited and typeset.

PLEASE CITE THIS ARTICLE AS DOI: 10.1063/1.50025490

an optical spectrum analyzer to record the peak powers of the output spectra. We first measured the off-resonant output power. Then, by finely tuning the laser wavelengths into the resonances, the output power decreases as they approach the resonances and the power stored in the resonator increases. When the current of the source meter reaches its maximum, it indicates the maximum power in the resonator at resonance. In detail, pump 1 was initially set to the wavelength of 1560.27 nm, and pump 2 was set to 1560.51 nm. With the method mentioned above, with a tuning step of 0.1 pm, we separately tuned both pumps into two adjacent resonances until the photocurrent reaches the maximum. Launching both pumps together rather than individually, produces additional thermal shifts in the resonance wavelengths of the cavity, and further fine-tuning is necessary when both pumps are launched. Here, instead of using a phase-locked loop to stabilize the pump frequency, we manually tuned the two pump wavelengths, using the TPA-induced photocurrent as a sensitive indicator for tuning the lasers into the resonances and producing the largest output OFC peaks.²⁶ We conducted the measurements with reverse bias voltages of 25 V, 10 V, and 0V. The p-i-n diode has a measured dark breakdown voltage of about 47 V, but we limited our experiment to only 25 V to avoid catastrophic breakdown damage to the device when it is optically pumped. The three spectra with the same pump powers are shown in FIG. 4. In the three spectra, we observed 11, 8, and 3 peaks. There were about 3.6 times more peaks when the 25 V bias voltage was applied. Including the loss of the resonator, the conversion efficiencies from the second pump to the first peak with the 25 V bias, 10 V bias, and 0 V bias were measured to be -24.2 dB, -28 dB, and -43.5 dB, respectively. The largest number of peaks and the highest conversion efficiency was achieved in the measurement with the 25 V bias. The coupled power of pump 1 was measured to be 0.3 mW. With the resonator enhancement factor of 32.3, the pump power in the cavity builds up to 9.7 mW in the racetrack ring waveguide. The asymmetrical comb spectra, as shown in FIG. 4, can be attributed to the mode coupling since no mode coupling would lead to symmetrical comb spectra to satisfy the energy conservation.^{5,7}

FIG. 5. Measured and simulated OFCs spectra at pump wavelengths of 1564 nm and reverse bias voltages of 25 V.

To verify the efficiency of using the mechanism of mode coupling in the normal dispersion regime of the high Q resonator to enhance the conversion efficiency of the OFC generation, we chose two pump wavelengths that are away from the mode coupling region to conduct the OFC generation measurement. As shown in FIG. 5, we chose the pump wavelength around 1564.2 nm. The loaded Q of the pump and was measured as 0.8×10^6 . We calculate the enhancement factor at this pump wavelength to be 22.7. With a coupled pump power of 0.9 mW, the power coupled into the resonator was 20.4 mW, which is higher than the above measurement. We applied reverse bias of 25 V and observed 8 peaks, as shown in FIG. 5. The measurement in the mode coupling region (FIG. 4a with the pump wavelength of 1560 nm) has 3 more peaks than the measurement outside the mode coupling region (FIG. 5). Including the loss of the resonator, the conversion efficiency

This is the author's peer reviewed, accepted manuscript. However, the online version of record will be different from this version once it has been copyedited and typeset.

PLEASE CITE THIS ARTICLE AS DOI: 10.1063/1.50025490

conversion was measured as -32.4 dB. There is an 8 dB reduction of the conversion efficiency of the OFC generation when pumped outside the mode coupling region. However, with higher circulating power inside the resonator, theoretical modeling shows that measurement around 1564 nm wavelength will have higher cavity power than at the 1560 nm resonance. However, in this measurement, which is away from the mode coupling regime, despite the higher pump powers circulating in the resonator, the number of the peaks and the conversion efficiency are lower than the measurement in the mode coupling regime. It thus confirms that the mode coupling significantly enhances the efficiency of the OFC generation.

Theoretically, the modified Lugiato-Lefever equation²⁷⁻³¹ including TPA, free carrier effects, and additional phase shift $\Delta\phi$ to the comb sideband in the frequency domain to approximate the effect of the mode coupling on the comb spectrum, may be used to describe the generation of frequency combs in multimode silicon resonators:

$$t_R \frac{\partial E(t, \tau)}{\partial t} = \left[-\frac{\alpha}{2} - \frac{\kappa}{2} - i\delta_0 - iL \frac{\beta_2}{2} \frac{\partial^2}{\partial \tau^2} + i\gamma L |E|^2 - \frac{\beta_{TPA} L}{2A_{eff}} |E|^2 - \frac{\sigma L}{2} (1 + i\mu) \langle N(t, \tau) \rangle + i(\Delta\phi) \right] E + \sqrt{\kappa} E_{in}, \quad (3a)$$

$$E_{in} = \sqrt{P_{in1}} + \sqrt{P_{in2}} \exp(-i2\pi f \tau), \quad (3b)$$

$$\frac{d \langle N(t) \rangle}{dt} = \frac{\beta_{TPA} |E|^4}{2\hbar\omega A_{eff}^2} - \frac{\langle N(t) \rangle}{\tau_{eff}}, \quad (3c)$$

where t_R , L and α are the cavity round-trip time, length and loss; κ is the power transmission coefficient; τ is the fast time; t is the slow time; δ_0 is the phase detuning of the pump laser; β_2 is the second-order dispersion parameter; γ is the Kerr coefficient; β_{TPA} is the TPA coefficient; A_{eff} is the effective area; σ is the free-carrier absorption cross-section; μ is the free-carrier dispersion parameter; $\langle N(t) \rangle = (1/t_R) \int_{-t_R/2}^{t_R/2} N(t, \tau) d\tau$ is the averaged free-carrier density; E_{in} is the external driving field; P_{in1} and P_{in2} are the powers of the two pumps; f is the frequency spacing between the two pumps; τ_{eff} is the free-carrier lifetime. The mode coupling may be modeled by an additional phase shift to the k -th mode.²⁷ Due to the additional phase shift from the mode coupling, the comb spectra are usually asymmetric²⁷, which are consistent with the measurements in FIG. 4 and FIG. 5. Either the split-step Fourier method or the Newton-Raphson method can be used to solve the above equations to describe the generation of Kerr frequency combs.^{27, 32-35} In the simulation, we used the split-step Fourier method with parameters: $L = 2.8$ mm; $\alpha = 0.25/0.57$ dB/cm, $\kappa = 0.0049/0.0144$, $P_{in1} = P_{in2} = 0.3/0.9$ mW at wavelength of 1560/1564 nm; $0 < \delta_0 < 0.02$; $\beta_2 = 100$ ps²/km; $n_2 = 5.5 \times 10^{-18}$ m²/W;^{36, 37} $\beta_{TPA} = 1.5 \times 10^{-11}$ m/W;³⁸ $A_{eff} = 4 \times 10^{-13}$ m²/W; $\sigma = 1.47 \times 10^{-18}$ m²/W;³⁹ $\mu = 7.5$;⁴⁰ $f = 29.6$

GHz; $\tau_{eff} = 15$ ns.^{41,42} Then we achieved the simulated OFCs spectra shown in FIG. 4d and FIG. 5b in correspondence to the experimental spectra of FIG. 4a and FIG. 5a. The experimental results agreed well with the theoretical simulations.

In conclusion, we experimentally studied OFC generation in a high-Q ($> 10^6$) multimode racetrack resonator and observed FWM with pump powers as low as $6 \mu\text{W}$ (at 25 V reverse bias) and $132 \mu\text{W}$ (with zero bias). The silicon racetrack resonator has a low propagation loss of 0.41 ± 0.16 dB/cm. Base on the multimode resonator platform, although the waveguide is in the normal dispersion regime with a wavelength range from 1400 nm to 1700 nm, we experimentally observed efficient six-order OFC generation with eleven peaks using two sub-milliwatt pumps and a 25 V reverse bias. The low pump power and high efficiency of the OFC generation can be explained by the mode coupling between the two modes in the multimode resonator, which can affect the local dispersion of the structure and even change its sign. Compared to the measurement without any bias, the application of 25 V bias produced 3.6 times more peaks and 12.1 dB enhancement in conversion efficiency. Compared to pump wavelengths tuned away from the mode coupling region, the pump wavelengths in the mode coupling region had 1.3 times more peaks and an 8 dB improvement in conversion efficiency. The experimental results were in accordance with theoretical estimations using the modified Lugiato-Lefever model. This work shows the potential for using multimode silicon devices for low-power nonlinear devices.

ACKNOWLEDGMENTS

This work was supported by Hong Kong Research Grants Council, General Research Fund (RGC, GRF) (14207117). We would like to thank Dr. Wen Zhou for designing the layout and IMEC for device fabrication and Dr. Jiayang Wu for help in simulation.

DATA AVAILABILITY

Data sharing is not applicable to this article as no new data were created or analyzed in this study.

REFERENCES

- ¹R. Salem, M. A. Foster, A. C. Turner, D. F. Geraghty, M. Lipson, and A. L. Gaeta, *Nat. Photonics* **2**, 35 (2008).
- ²W. Mathlouthi, H. Rong, and M. Paniccia, *Opt. Express* **16**, 16735-16745 (2008).
- ³R. Salem, M. A. Foster, A. C. Turner, D. F. Geraghty, M. Lipson, and A. L. Gaeta, *Opt. Lett.* **33**, 1047-1049 (2008).
- ⁴M. A. Foster, A. C. Turner, J. E. Sharping, B. S. Schmidt, M. Lipson, and A. L. Gaeta, *Nature* **441**, 960 (2006).
- ⁵Y. Liu, Y. Xuan, X. Xue, P.-H. Wang, S. Chen, A. J. Metcalf, J. Wang, D. E. Leaird, M. Qi, and A. M. Weiner, *Optica* **1**, 137-144 (2014).
- ⁶X. Xue, Y. Xuan, P. H. Wang, Y. Liu, D. E. Leaird, M. Qi, and A. M. Weiner, *Laser Photonics Rev.* **9**, L23-L28 (2015).
- ⁷A. Savchenkov, A. Matsko, W. Liang, V. Ilchenko, D. Seidel, and L. Maleki, *Opt. Express* **20**, 27290-27298 (2012).
- ⁸S. A. Miller, Y. Okawachi, S. Ramelow, K. Luke, A. Dutt, A. Farsi, A. L. Gaeta, and M. Lipson, *Opt. Express* **23**, 21527-21540 (2015).
- ⁹X. Xue, Y. Xuan, Y. Liu, P.-H. Wang, S. Chen, J. Wang, D. E. Leaird, M. Qi, and A. M. Weiner, *Nat. Photonics* **9**, 594-600 (2015).

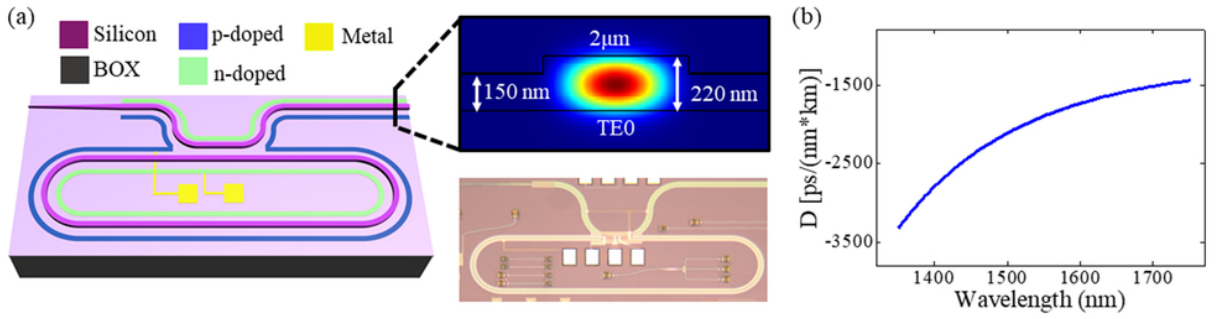
This is the author's peer reviewed, accepted manuscript. However, the online version of record will be different from this version once it has been copyedited and typeset.

PLEASE CITE THIS ARTICLE AS DOI: 10.1063/1.50025490

- ¹⁰A. Kordts, M. H. Pfeiffer, H. Guo, V. Brasch, and T. J. Kippenberg, *Opt. Lett.* **41**, 452-455 (2016).
- ¹¹P. Del'Haye, O. Arcizet, M. L. Gorodetsky, R. Holzwarth, and T. J. Kippenberg, *Nat. Photonics* **3**, 529 (2009).
- ¹²I. S. Grudin, L. Baumgartel, and N. Yu, *Opt. Express* **21**, 26929-26935 (2013).
- ¹³T. Herr, V. Brasch, J. Jost, I. Mirgorodskiy, G. Lihachev, M. Gorodetsky, and T. Kippenberg, *Phys. Rev. Lett.* **113**, 123901 (2014).
- ¹⁴A. C. Turner, C. Manolatou, B. S. Schmidt, M. Lipson, M. A. Foster, J. E. Sharping, and A. L. Gaeta, *Opt. Express* **14**, 4357-4362 (2006).
- ¹⁵X. Ji, F. A. Barbosa, S. P. Roberts, A. Dutt, J. Cardenas, Y. Okawachi, A. Bryant, A. L. Gaeta, and M. Lipson, *Optica* **4**, 619-624 (2017).
- ¹⁶Y. Zhang, X. Hu, D. Chen, L. Wang, M. Li, P. Feng, X. Xiao, and S. Yu, *Opt. Lett.* **43**, 1586-1589 (2018).
- ¹⁷S. Signorini, M. Mancinelli, M. Borghi, M. Bernard, M. Ghulinyan, G. Pucker, and L. Pavesi, *Photonics Res.* **6**, 805-814 (2018).
- ¹⁸R. R. Kumar, Y. Wang, Y. Zhang, and H. K. Tsang, *JOSA B* **37**, 2231-2237 (2020).
- ¹⁹S. Paesani, M. Borghi, S. Signorini, A. Maños, L. Pavesi, and A. Laing, *Nat. Commun.* **11**, 1-6 (2020).
- ²⁰Y. Zhang, W. Zhou, D. Yi, Z. Zhang, Y. Tong, R. R. Kumar, Y. Wang, and H. K. Tsang, in *Asia Communications and Photonics Conference* (Optical Society of America, 2019), p. M4A. 240.
- ²¹M. Ghulinyan, F. R. Manzano, N. Prtljaga, M. Bernard, L. Pavesi, G. Pucker, and I. Carusotto, *Phys. Rev. A* **90**, 053811 (2014).
- ²²M. Bernard, F. R. Manzano, L. Pavesi, G. Pucker, I. Carusotto, and M. Ghulinyan, *Photonics Res.* **5**, 168-175 (2017).
- ²³W. Bogaerts, P. De Heyn, T. Van Vaerenbergh, K. De Vos, S. Kumar Selvaraja, T. Claes, P. Dumon, P. Bienstman, D. Van Thourhout, and R. Baets, *Laser Photonics Rev.* **6**, 47-73 (2012).
- ²⁴L.-W. Luo, G. S. Wiederhecker, J. Cardenas, C. Poitras, and M. Lipson, *Opt. Express* **19**, 6284-6289 (2011).
- ²⁵M. Borselli, T. J. Johnson, and O. Painter, *Opt. Express* **13**, 1515-1530 (2005).
- ²⁶P. Del'Haye, O. Arcizet, A. Schliesser, R. Holzwarth, and T. J. Kippenberg, *Phys. Rev. Lett.* **101**, 053903 (2008).
- ²⁷X. Xue, M. Qi, and A. M. Weiner, *Nanophotonics* **5**, 244-262 (2016).
- ²⁸M. Haelterman, S. Trillo, and S. Wabnitz, *Opt. Commun.* **91**, 401-407 (1992).
- ²⁹M. Liu, L. Wang, Q. Sun, S. Li, Z. Ge, Z. Lu, W. Wang, G. Wang, W. Zhang, and X. Hu, *Photonics Res.* **6**, 238-243 (2018).
- ³⁰R. K. Lau, M. R. Lamont, Y. Okawachi, and A. L. Gaeta, *Opt. Lett.* **40**, 2778-2781 (2015).
- ³¹H. Guo, M. Karpov, E. Lucas, A. Kordts, M. H. Pfeiffer, V. Brasch, G. Lihachev, V. E. Lobanov, M. L. Gorodetsky, and T. J. Kippenberg, *Nat. Phys.* **13**, 94-102 (2017).
- ³²S. Coen, H. G. Randle, T. Sylvestre, and M. Erkintalo, *Opt. Lett.* **38**, 37-39 (2013).
- ³³S. Coen, and M. Erkintalo, *Opt. Lett.* **38**, 1790-1792 (2013).
- ³⁴Y. K. Chembo, and C. R. Menyuk, *Phys. Rev. A* **87**, 053852 (2013).
- ³⁵P. Parra-Rivas, D. Gomila, M. A. Matias, S. Coen, and L. Gelens, *Phys. Rev. A* **89**, 043813 (2014).
- ³⁶M. Dinu, F. Quochi, and H. Garcia, *Appl. Phys. Lett.* **82**, 2954-2956 (2003).
- ³⁷H. K. Tsang, C. Wong, T. Liang, I. Day, S. Roberts, A. Harpin, J. Drake, and M. Asghari, *Appl. Phys. Lett.* **80**, 416-418 (2002).
- ³⁸A. D. Bristow, N. Rotenberg, and H. M. Van Driel, *Appl. Phys. Lett.* **90**, 191104 (2007).
- ³⁹R. Soref, and J. Lorenzo, *IEEE J. Quantum Electron.* **22**, 873-879 (1986).
- ⁴⁰R. Soref, and B. Bennett, *IEEE J. Quantum Electron.* **23**, 123-129 (1987).
- ⁴¹T. Liang, and H. Tsang, *Appl. Phys. Lett.* **84**, 2745-2747 (2004).
- ⁴²H. Rong, A. Liu, R. Nicolaescu, M. Paniccia, O. Cohen, and D. Hak, *Appl. Phys. Lett.* **85**, 2196-2198 (2004).

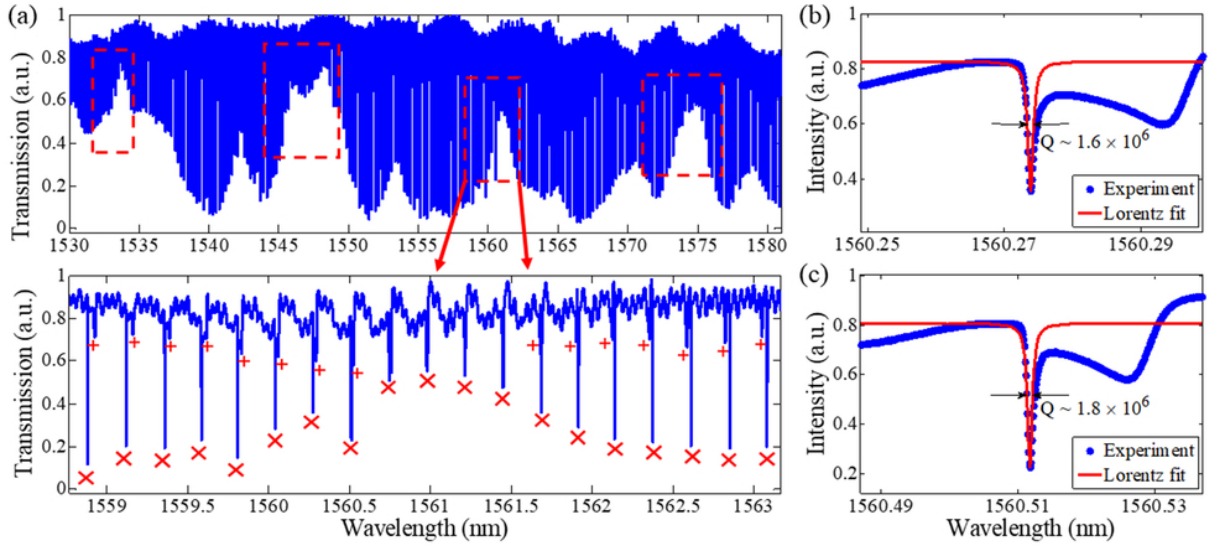
This is the author's peer reviewed, accepted manuscript. However, the online version of record will be different from this version once it has been copyedited and typeset.

PLEASE CITE THIS ARTICLE AS DOI: 10.1063/1.50025490

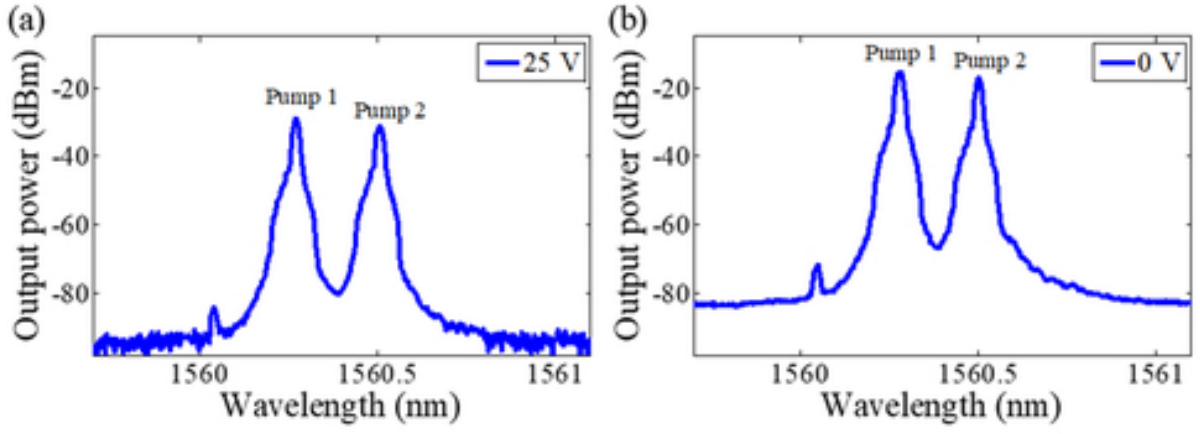


This is the author's peer reviewed, accepted manuscript. However, the online version of record will be different from this version once it has been copyedited and typeset.

PLEASE CITE THIS ARTICLE AS DOI: 10.1063/1.50025490

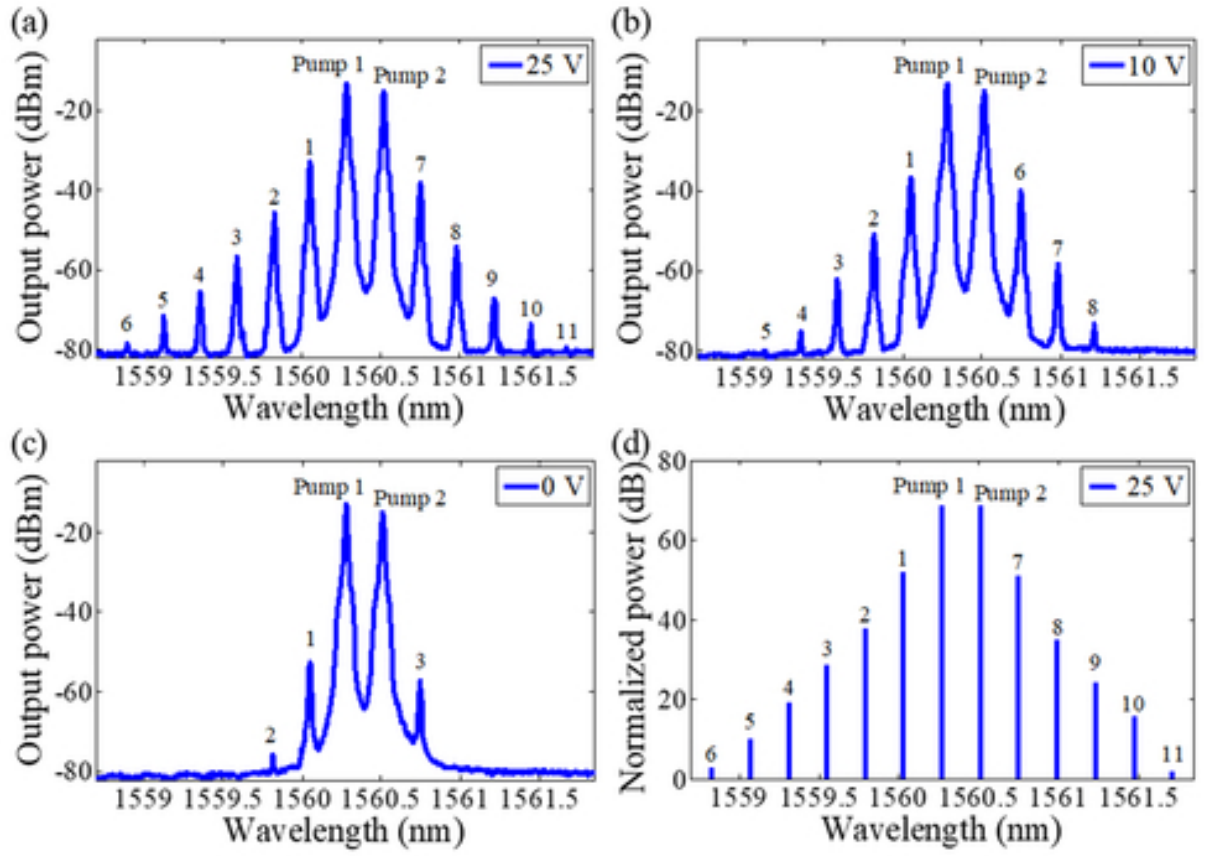


This is the author's peer reviewed, accepted manuscript. However, the online version of record will be different from this version once it has been copyedited and typeset.
 PLEASE CITE THIS ARTICLE AS DOI: 10.1063/5.0025490



This is the author's peer reviewed, accepted manuscript. However, the online version of record will be different from this version once it has been copyedited and typeset.

PLEASE CITE THIS ARTICLE AS DOI: 10.1063/1.50025490



This is the author's peer reviewed, accepted manuscript. However, the online version of record will be different from this version once it has been copyedited and typeset.

PLEASE CITE THIS ARTICLE AS DOI: 10.1063/1.50025490

